

Evolution of the magnetism of $\text{Tb}(\text{Co}_x\text{Ni}_{1-x})_2\text{B}_2\text{C}$

M. ElMassalami,¹ H. Takeya,² A. M. Gomes,¹ T. Paiva,¹ and R. R. dos Santos¹

¹*Instituto de Física, Universidade Federal do Rio de Janeiro,
Caixa Postal 68528, 21941-972 Rio de Janeiro, Brazil, and*

²*National Institute for Materials Science, 1-2-1 Sengen, Tsukuba, Ibaraki 305-0047, Japan,
(Dated: Version 6 – July 4, 2012)*

Abstract

The magnetic properties of polycrystalline $\text{Tb}(\text{Co}_x\text{Ni}_{1-x})_2\text{B}_2\text{C}$ ($x = 0.2, 0.4, 0.6, 0.8$) samples were probed by magnetization, specific heat, *ac* susceptibility, and resistivity techniques. For $x \neq 0.4$, the obtained curves are consistent with the features expected for the corresponding magnetic modes, namely $\vec{k}_1 = (0.55, 0, 0)$ at $x = 0$; $\vec{k}_2 = (1/2, 0, 1/2)$ at $x = 0.2$; $\vec{k}_3 = (0, 0, 1/3)$ at $x = 0.6$, and $\vec{k}_4 = (0, 0, 0)$ at $x = 0.8$ and 1. For $x = 0.4$, even though the neutron diffraction indicates a \vec{k}_2 mode, but with a reduced magnetic moment, the magnetization, the *ac* susceptibility, and resistivity indicate two magnetic events; furthermore, deviation from Curie-Weiss behavior is observed below 150 K for this sample. These features, together with the evolution of both magnetic moment and critical temperature, are attributed to an interplay between competing magnetic couplings; for the particular $x = 0.4$ case, additional factors such as crystalline electric field effects may be in operation.

PACS numbers: 74.70.Dd, 71.27.+a, 75.50.-y, 75.50.Cc, 75.30.Fv, 75.20.Hr

I. INTRODUCTION

The crystal structure of various families of compounds consists of magnetic layers that are separated by nonmagnetic spacers. As in most cases, the interlayer couplings in such arrangement are taken to be mediated by extended electronic orbitals; therefore, a variation in electronic parameters of the spacers is expected to have a profound influence on the magnetism, as well as on the overall physical properties of the whole system. Such influence is most dramatically manifested whenever the energy of the magnetic coupling is close to that of the electronic interactions such as pairing or electron-phonon interactions. Indeed, striking manifestations are evident in the magnetic and transport properties of layered materials such as magnetic multilayers, high- T_c cuprates, pnictides superconductors, intermetallic magnetic superconductors, and heavy fermion compounds.

The intermetallic borocarbides $RT_2\text{B}_2\text{C}$ (R is a rare earth atom with $4f$ moment, and T is an unpolarized transition metal atom) comprise one of these magnetically layered families wherein the magnetic RC are stacked on the nonmagnetic $T_2\text{B}_2$ spacers, forming an $\cdots RC-T_2\text{B}_2-RC \cdots$ pile.^{1,2} The electronic properties of the $T_2\text{B}_2$ spacers are crucial to the determination of the overall physical properties, as manifested by the surge of a wealth of exotic phenomena; see Refs.1–4, and references therein. Of particular interest to the present study is the influence that the electronic properties exercise on the stabilization of the ground-state magnetic structure. This is best illustrated by how the magnetic arrangement of the Tb sublattice for different $\text{Tb}(\text{Co}_x\text{Ni}_{1-x})_2\text{B}_2\text{C}$ compositions is controlled by the relative abundance of Ni and Co, x :⁵ the longitudinal spin density wave, LSDW, $\vec{k}_1 = (0.55, 0, 0)$ state at $x = 0$ is transformed into a collinear $\vec{k}_2 = (1/2, 0, 1/2)$ antiferromagnetic, AFM, state

at $x = 0.2, 0.4$; then into a transverse *c*-axis modulated $\vec{k}_3 = (0, 0, 1/3)$ mode at $x = 0.6$, and finally into a simple ferromagnetic, FM, structure, $\vec{k}_4 = (0, 0, 0)$, at $x = 0.8$ and 1.0 (see Table I).

This tuning in of magnetic modes by a simple variation of x highlights the importance of electronic band structures (which are dominated by the spacer 3d orbitals).^{6–10} indeed, the generalized susceptibility calculations of Rhee *et al.*¹¹ predict a variety of magnetic modes, one of which was verified only recently.⁵ An alternative theoretical analysis was proposed by Bertussi *et al.*,¹² based on an effective microscopic model in which the interplay between local moments ordering and superconductivity is explicitly taken into account. This interplay, as well as the specific layering character of borocarbides¹³ have been tested in one spatial dimension (1D), which is amenable to unbiased calculations, and, as it turned out, the key element consists of conduction electrons being mediators of both pairing and magnetic coupling. In this way, a phase diagram relating the magnetic coupling to a succession of magnetic modes is established,¹² and this phase diagram is found to be in fair agreement with the experimental observations.⁵

The success of these theoretical approaches is impressive, considering that the calculations of Rhee *et al.* do not admit pairing interactions, while those for the effective microscopic model have so far been carried out only in 1D. In both cases, however, theoretical results are only available for the ground state ($T = 0$), thus not covering the rich features of thermodynamic properties which, for $R(T_x\text{M}_{1-x})_2\text{B}_2\text{C}$ ($T, M = 3d$ atoms), have been extensively studied (see, e.g., Refs. 1, 2, and references therein). Evidently, an investigation of the above mentioned influence of the spacer on both the thermodynamic properties and magnetic structures would be a welcome contribution for the understanding of the mechanisms behind

TABLE I: Selected magnetic properties of $\text{Tb}(\text{Co}_x\text{Ni}_{1-x})_2\text{B}_2\text{C}$ (adapted from Ref. 5). μ_{ND} (μ_{M}) is the zero-field (90 kOe) value obtained from neutron diffraction (magnetization isotherm). $T_{\text{cr}}(x)$ is the critical point which is taken from each experimental curve. As seen, except for $x = 0.4$, the obtained transition point decreases monotonically with x , and, interestingly, tracks the behavior of the unit-cell volume;⁵ this emphasizes the dependence of both on the electronic structure.

x	0 ^a	0.2	0.4	0.6	0.8	1.0 ^b
structure	LSDW	AFM	AFM	TSDW	FM	FM
\vec{k}	(0.55, 0, 0)	(1/2, 0, 1/2)	(1/2, 0, 1/2)	(0, 0, 1/3)	(0, 0, 0)	(0, 0, 0)
$ \vec{\mu} _{\text{ND}} (\mu_B)$	7.8	7.6(1)	3.7(2)	8.5(2)	8.7(2)	7.6
$ \vec{\mu} _{\text{M}(90 \text{ kOe})} (\mu_B)$	7.4(1)	4.1(1)	7.6(2)	7.7(1)	7.6(1)	7.2
T_{cr} (K) from $C(T, x)$	15 ^c	10.2(2)	$T_2 = 4.8(3) \text{ K}^d$	7.6(3)	5.9(2)	6.6 ^e
" " $\chi_{dc}(T, x)$	-	10.4(2)	$T_1 = 11.0(2) \text{ K}, T_2 = 4.3(3) \text{ K}$	7.6(2)	5.9(2)	-
" " $\chi_{ac}(T, x)$	-	10.3(2)	$T_1 = 11.8(2) \text{ K}, T_2 = 4.0(2) \text{ K}$	7.6(2)	5.9(2)	-

^aRef.14

^bRef.15.

^csee Ref.14. The specific heat of $\text{TbNi}_2\text{B}_2\text{C}$ from the present batch peaks at $T_p = 13.2(2) \text{ K}$

^dOnly one event can be discerned [see text and Fig. 4(b)]

^eRef.15. The specific heat of $\text{TbCo}_2\text{B}_2\text{C}$ from the present batch peaks at $T_p = 5.6(3) \text{ K}$

many features occurring in the above layered systems (e.g., superconductivity in cuprates, heavy fermions, and pnictides materials; coexistence of superconductivity and magnetic order in magnetic superconductors, giant magnetoresistance, etc.). As far as the borocarbides are concerned, such investigation would motivate and guide further theoretical analyses, in particular those contemplating a unified description of the observed magnetic and superconducting properties. In pursuit of these objectives, here we report on the evolution of the magnetic properties of $\text{Tb}(\text{Co}_x\text{Ni}_{1-x})_2\text{B}_2\text{C}$ ($x = 0.2, 0.4, 0.6, 0.8$) when control parameters (such as x , temperature, field, frequency) are varied over a wide measuring range; we use magnetization, specific heat, ac -susceptibility, and resistivity techniques. Our findings will be discussed in terms of the influence of the electronic properties of $(\text{Co}_x\text{Ni}_{1-x})_2\text{B}_2$ on the observed behavior.

The layout of the paper is as follows. In Sec. II we outline the measuring techniques employed, while in Sec. III the results are analyzed. Section IV closes the paper with discussions and conclusions.

II. EXPERIMENTAL

The polycrystalline samples used in this work were the same as the ones used previously⁵ for collecting neutron diffractograms. The only difference is that the diffractograms and ac susceptibility have been collected on powdered samples, while the magnetization and specific heat had been measured on the same small solid piece. This choice of solid form, instead of a powder one, is dictated by the requirement of the specific-heat set-up. But this introduces those well-known strong anisotropic features;¹⁶ as a consequence, the shapes of the field-dependent curves differ considerably from those obtained

on powdered or single crystal samples; nevertheless, the analysis and interpretation of these curves are straightforward (see below). It is worth adding that single-crystal studies on this series, though it is highly desirable, would not invalidate any of the results obtained in this work.

Magnetization and dc susceptibility (M , $\chi_{dc} = M/H$, $2 < T < 20 \text{ K}$, $H \leq 90 \text{ kOe}$) were measured on an extraction-type magnetometer, while the specific heats (C , $2 < T < 40 \text{ K}$ and $H = 0, 30 \text{ kOe}$) were measured on a relaxation-type calorimeter. AC susceptibilities ($\chi_{ac} = \partial M / \partial H$, $f \leq 10 \text{ kHz}$, $2 \leq T \leq 20 \text{ K}$, $h_{ac} \leq 10 \text{ Oe}$, $H \leq 90 \text{ kOe}$) were measured on a mutual-induction susceptometer.

Longitudinal magnetoresistivity, $\rho(T, H, I || H)$ of a polycrystalline $x = 0.4$ sample was measured by a conventional, home-made, in-line four-point magnetoresistometer ($0 \leq H \leq 50 \text{ kOe}$, $1.8 \leq T \leq 300 \text{ K}$, and $0.1 \leq I \leq 1 \text{ mA}$). The residual resistivity ratio, $RRR \equiv \rho(300\text{K})/\rho(1.8\text{K})$, was found to be ~ 1 ; this large value is attributed to the relatively large temperature-independent scattering, arising from the random distribution of Co/Ni atoms.

Most measurements, in particular those on the $x = 0.4$ sample, exhibit strong hysteresis effects. In order to avoid any complication arising from the associated history effect, samples were heated up to 50 K (or even higher temperatures) between successive measurements. Due to these hysteresis effects, as well as to the widespread and, sometimes, ill-defined shape of the peak associated with magnetic order, the identification of a unique transition point was found to be difficult. Accordingly, two definitions of the critical temperature were adopted (see Table I): (i) $T'_{\text{cr}}(x)$ is defined as the point where $C(T, x)$ starts to increase, or the entropy, $S(T, x)$, starts to deviate downwards away from the high- T extrapolation, though in some cases $T'_{\text{cr}}(x)$ is manifested as a shoulder;

(ii) the peak-maximum, $T_p(x)$, of $C(T, x)$, $\rho(T, x = 0.4)$, $\chi_{dc}(T, x)$, and $\chi_{ac}(T, x)$. The difference between $T'_{cr}(x)$ and $T_p(x)$ is most probably related to atomic distributions. At any rate, these identifications would not cause any loss of generality or modify the conclusions reached.

III. RESULTS AND ANALYSES

A. Magnetization

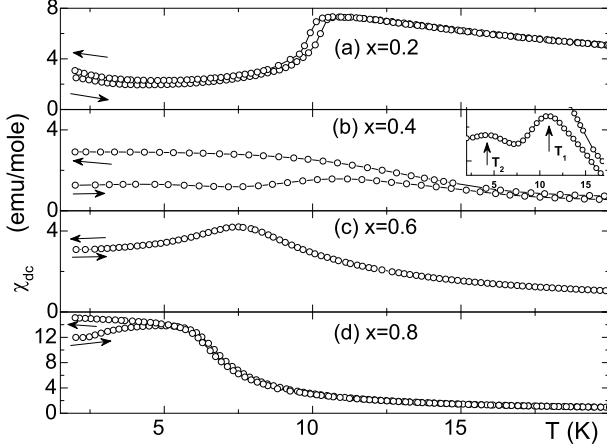


FIG. 1: Magnetic susceptibilities ($\chi_{dc} = M/H$) for $\text{Tb}(\text{Co}_x\text{Ni}_{1-x})_2\text{B}_2\text{C}$. For the zero-field curves of $x = 0$ and 1, see Refs. 16 and 15, respectively. Zero-field-cooled and field-cooled measurements ($H = 200$ Oe) were carried out on warming and cooling branch, respectively. Inset: expansion of the $x = 0.4$ curve, showing the T_1 and T_2 events on the warming-up branch (see text).

Representative $\chi_{dc}(T, x)$ curves are shown in Fig. 1. $\chi_{dc}(T, x = 0)$ of $\text{TbNi}_2\text{B}_2\text{C}$ (not shown) indicates an AFM-type behavior with a weak FM anomaly at lower temperatures.¹⁶ Similarly, $\chi_{dc}(T, x = 1)$ of $\text{TbCo}_2\text{B}_2\text{C}$ (not shown) exhibits the onset of the FM state together with the characteristic ZFC and FC branches.¹⁵ Some data for these two limiting compositions have been collected in Table I. $\chi_{dc}(T, x)$ of each intermediate composition evolves between these two limits. Based on the magnetic structures identified in Ref. 5, one is able to associate the shape of $\chi_{dc}(T, x = 0.2)$ with the \vec{k}_2 AFM mode, and those of $\chi_{dc}(T, x = 0.6, 0.8)$ with the \vec{k}_3 and \vec{k}_4 modes. By contrast, the shape of $\chi_{dc}(T, x = 0.4)$ is distinctly different, and manifests strong hysteresis effects: during the warming branch, two events appear (see inset of Fig. 1), one at $T_1 = 11.0 \pm 0.2$ K, and another at $T_2 = 4.3 \pm 0.3$ K.

Typical $M(2\text{ K}, H, x)$ isotherms are shown in Fig. 2(a)-(e); in the low-field regime, these confirm the AFM-type character of the $x \leq 0.4$ samples, and the FM behavior of the $x \geq 0.8$ compositions. In the $H \rightarrow 90$ kOe range, the saturated feature of the magnetic moments is

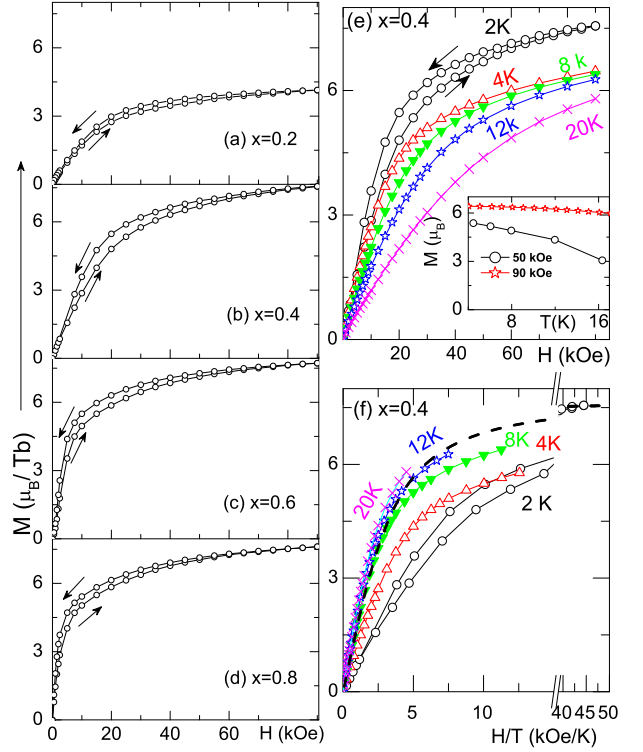


FIG. 2: (Color online) Magnetization isotherms of $\text{Tb}(\text{Co}_x\text{Ni}_{1-x})_2\text{B}_2\text{C}$: (a) $x = 0.2$, (b) 0.4, (c) 0.6, and (d) 0.8, measured at $T = 2$ K. (e) Magnetization isotherms of the $x = 0.4$ sample, measured at 2, 4, 8, 12 and 20 K. Inset: Thermal evolution of the $M(H, x = 0.4)$, $H = 50, 90$ kOe, indicating the absence of any event, neither at T_1 nor at T_2 . (f) These same curves are plotted against H/T . The dashed line represents the calculated Brillouin function ($g = 1.5$, $J = 6$) which is scaled to the saturation moment of $7.6 \mu_B$.

clearly manifested, and the evaluated values are shown in Table I. In comparison with $\bar{\mu}_{\text{ND}}$, $|\bar{\mu}|_{M(90\text{ kOe})}(x)$ for $x = 0.0, 0.6, 0.8$ and 1.0 are in reasonable agreement, but those for $x = 0.2$ and 0.4 differ significantly. For $x = 0.2$, the anomalously lower value of $|\bar{\mu}|_{M(90\text{ kOe})}$ is attributed to the strong anisotropic character of this sample, which hinders the saturation to full moment value; indeed, full saturation is recovered when the magnetization is measured on a powdered $x = 0.2$ sample. On the other hand, high field data for $x = 0.4$ indicate an almost fully saturated parallel component. This suggests that the process leading to a reduction in the zero-field $\bar{\mu}_{\text{ND}}$ is no longer effective upon application of a 90 kOe field; more on this below. In order to follow this process, we have measured various $M(T, H, x = 0.4)$ curves; see Fig. 2(e). When these are plotted as functions of H/T [Fig. 2(f)], three different regimes can be identified. At high temperatures, all curves collapse very closely onto the Brillouin function, consistently with a paramagnetic state. Interestingly, upon lowering the temperature this behavior changes over near T_1 , when the curves start deviating downwards away from the Brillouin function, signaling

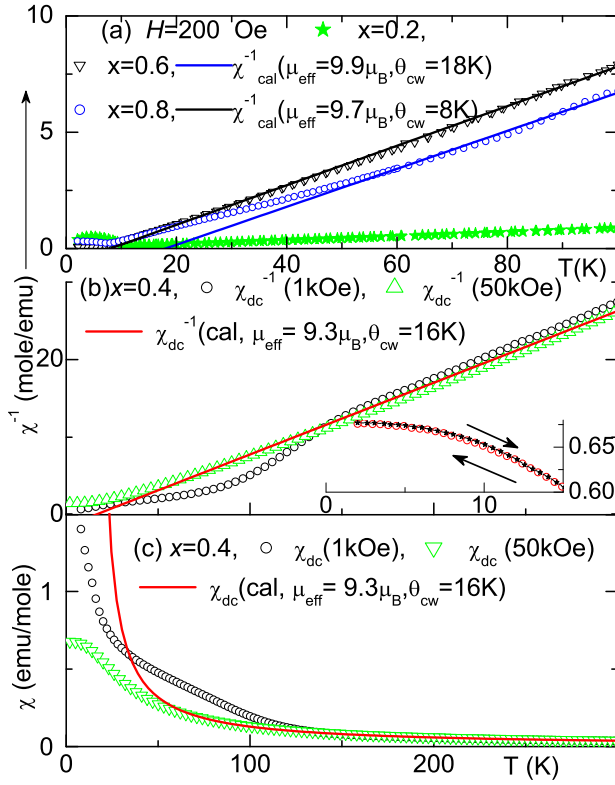


FIG. 3: (Color online) (a) Thermal evolution of the inverse dc susceptibility of $\text{Tb}(\text{Co}_x\text{Ni}_{1-x})_2\text{B}_2\text{C}$, $x = 0.2, 0.6$, and 0.8 for $H = 200$ Oe; the solid lines represent the reciprocal of $\chi_{dc}(T) = 0.125 \mu_{\text{eff}}^2 / (T - \theta_{CW})$ emu/mole where μ_{eff} (in μ_B) is the effective moment, while θ_{CW} (in K) is the Curie-Weiss temperature. The deviation of the $x = 0.2$ curve is related to the preferred orientation (see text). (b) Same as (a), but for the $x = 0.4$ sample, and for both $H = 1$ kOe and 50 kOe. (c) Same data as (b), but now is the susceptibility vs. temperature. Inset: $\chi_{dc}(T, x = 0.4, H = 50 \text{ kOe})$ on warming (stars) and cooling (circles) branch, indicating the reduction of hysteresis effects.

the appearance of a non-zero Weiss molecular field. This persists down to $T \approx T_2$, below which $M(H/T)$ shows appreciable hysteresis, and saturation is reached at higher H/T values. Two interesting examples of the thermal evolution of the isofield magnetization are shown in the inset of Fig. 2(e): when fields of 50 and 90 kOe are applied, the moment is almost saturated, and its thermal evolution shows a smooth monotonic reduction, with no sign of anomaly at or below T_1 or T_2 ; manifestations of these events only appear at lower fields.

The high-temperature susceptibility for the $x = 0.4, 0.6$, and 0.8 samples show a well defined Curie-Weiss (CW) behavior [Figs.3(a) and (b)], with $\mu_{\text{eff}}(x = 0.4) = 9.3 \mu_B$, $\mu_{\text{eff}}(x = 0.6) = 9.9 \mu_B$, and $\mu_{\text{eff}}(x = 0.8) = 9.8 \mu_B$; these are very close to the theoretical value of $9.72 \mu_B$ for the free Tb^{3+} ion. By contrast, no such agreement is observed for $x = 0.2$: this is related to the strong preferred orientation [see the discussion of Fig. 2(a)]. Nonetheless, it is important to notice from Figs.

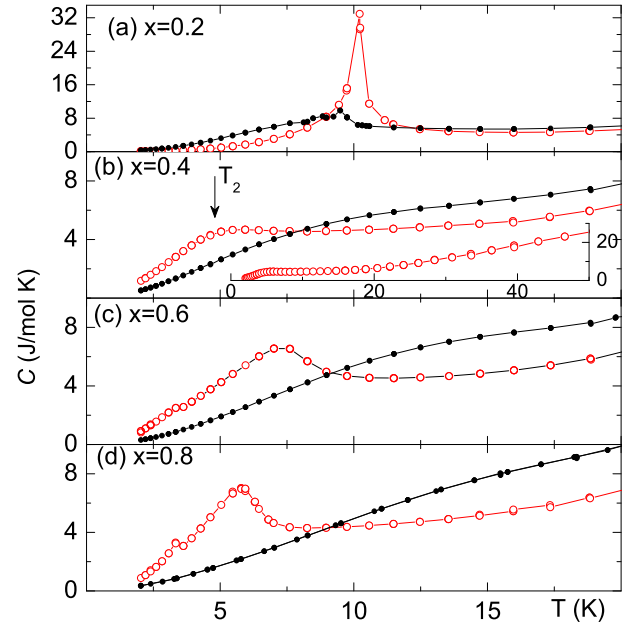


FIG. 4: (Color online) Specific heat of $\text{Tb}(\text{Co}_x\text{Ni}_{1-x})_2\text{B}_2\text{C}$. The scales of the vertical axes are not the same. Open symbols: measured at $H = 0$; closed symbols: measured at $H = 30$ kOe. Inset: $C(T, H = 0, x = 0.4)$ over a wider temperature range. In panel (b), while the wide shoulder can be attributed to T_2 event, there are no visible manifestation of the T_1 event. The weak shoulder appearing at ~ 4 for the $x = 0.6$ and 0.8 curves is attributed to the same anomalous feature reported earlier in $\text{TbCo}_2\text{B}_2\text{C}$ (see Ref. 15).

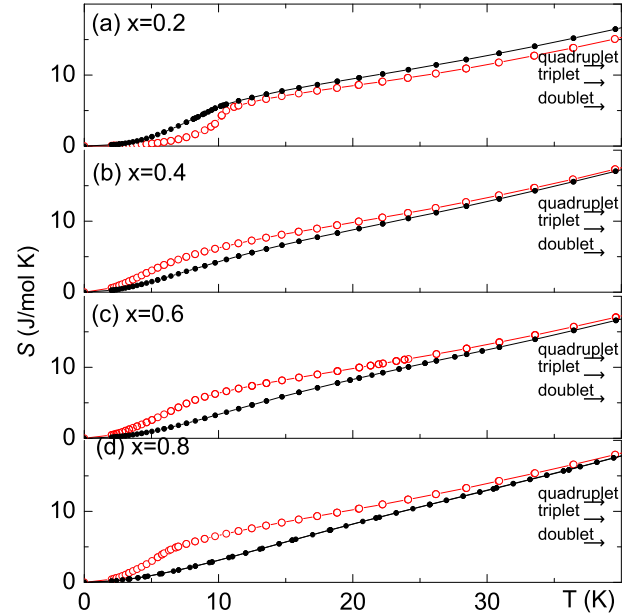


FIG. 5: (Color online) Thermal evolution of the calculated entropy of $\text{Tb}(\text{Co}_x\text{Ni}_{1-x})_2\text{B}_2\text{C}$. The horizontal arrows indicate the entropy associated with a doublet, triplet, and quadruplet state.

3(b) and (c) that, below 150 K, $\chi_{dc}(T, x = 0.4, 1 \text{ kOe})$ deviates sharply from the high-temperature CW behavior, with strong hysteresis effects developing at lower temperatures, as displayed in Fig. 1(b); upon application of a 50 kOe field, the CW behavior of $\chi_{dc}(T, x = 0.4, 50 \text{ kOe})$ is observed to survive at much lower temperatures [Figs. 3(b) and (c)], and no hysteresis effects are manifested [inset of 3(b)].

B. Specific Heat

Specific heat curves, $C(T, x)$, are shown in Fig. 4, while the calculated entropy, $S(T, x)$ is shown in Fig. 5. At such temperatures, the magnetic (not the weak electronic and lattice) contribution is dominant. The overall features of these $C(T, x, H = 0)$ curves depend strongly on the underlying crystal and magnetic structures. For instance, Fig. 4 indicates that the $x = 0.2$ displays a sharp peak near $T_p(x = 0.2) = 10 \text{ K}$, in marked contrast to all other concentrations; this is attributed to the influence of a strong magneto-elastic coupling, which causes the magnetic phase transition to be accompanied by an orthorhombic structural distortion.^{17–19}

The thermal evolutions of $C(T, 30 \text{ kOe})$ for all compositions (except for $x = 0.2$) are similar and featureless. Based on the magnetic phase diagrams of $\text{TbCo}_2\text{B}_2\text{C}$ (Ref. 15) and $\text{TbNi}_2\text{B}_2\text{C}$ (Ref. 16), a field of 30 kOe applied along the a axis would force the Tb moments towards saturation. Consequently, the magnetic contribution to the low- T (i.e., $T < T_{cr}$) specific heat of each composition is due to spin-wave excitations from similar saturated FM states. On the other hand, for $T > T_{cr}$ the contributions are due to excitations from similar CEF-split levels. The weak peak at $T \approx 9 \text{ K}$ for $x = 0.2$ suggests that for this particular solid sample (with strongly preferred orientation), the saturation field is higher than 30 kOe; this feature is consistent with the above-mentioned anisotropy-limited saturation of the magnetic moment [see Fig. 2(a)] and the anomalous CW behavior of Fig. 3(a).

Figure 5 indicates that the thermal evolution of $S(T < T_{cr}, x \geq 0.4, H = 30 \text{ kOe})$ is very different from that of $S(T < T_{cr}, x < 0.4, H = 30 \text{ kOe})$: for $x > 0.4$, the applied field reduces the thermally-induced randomness in the FM states, as well as in the c -axis modulated mode; similarly, for $x = 0.4$ the magnetic disorder is greatly reduced (see below). By contrast, for $x < 0.4$, the disorder of the AFM-type structure is increased when a smaller H is applied.

Figure 5 also shows that $S(T, x, 30 \text{ kOe})$ increases smoothly with T , reaching the calculated contributions of a doublet, triplet, or a quadruplet state and afterwards reaches 17–18 J/moleK at 40 K. It is noteworthy that: (i) $S(40 \text{ K})$ is almost the same for all concentrations, and independent of H , indicating that the entropy is predominantly due to the single-ion character of Tb^{3+} ; and (ii) a slight discrepancy between $S(40 \text{ K}, 0 \text{ kOe})$ and $S(40 \text{ K},$

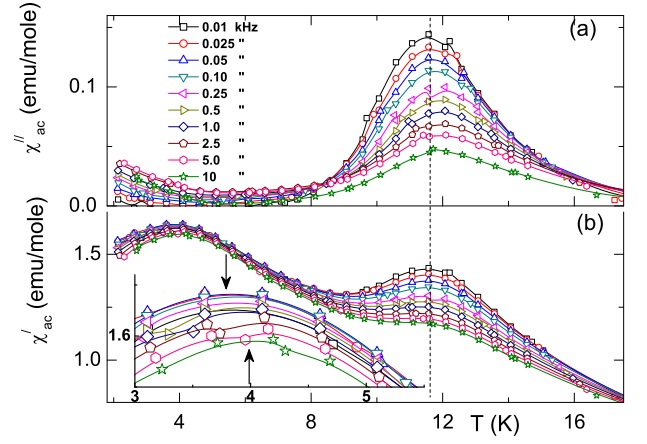


FIG. 6: (Color online) Thermal evolution of the ac susceptibility for the $x = 0.4$ sample, taken at $h_{ac} = 10 \text{ Oe}$, and various frequencies. (a) χ''_{ac} : the out-of-phase component; (b) χ'_{ac} : the in-phase component. The vertical dashed line emphasizes the absence of a frequency-dependent variation in the peak position (though an intensity reduction is evident). Inset: an expansion of the lower peaks showing a 10% reduction in the peak position for four decade frequency variation (denoted by the short vertical arrows).

30 kOe) is present solely for $x = 0.2$, which is related to the *zero-field* tetragonal-to-orthorhombic distortion occurring at this concentration; a 30 kOe field suppresses such a distortion and, as a consequence, eliminates the corresponding contribution.

Finally, $C(T, x = 0.4)$ of Fig. 4(b) displays a shoulder which, upon comparison with Fig. 1(b), can be related to the T_2 event. By contrast, no sign or anomaly, which can be associated with the T_1 event, is exhibited; this suggests that the amount of the involved entropy is so small that no perceptible change is evident.

C. AC susceptibility

The discussion so far has unveiled a rather subtle behavior of the $x = 0.4$ sample, hence deserving a more thorough analysis. In order to explore whether there are any dynamic features accompanying its anomalous magnetic behavior, we have measured its ac susceptibility as a function of frequency (f), H , and T : these are shown in Figs. 6 to 8. Indeed there are strong and unique dynamic signatures which are fully emphasized when compared to the conventional ac susceptibility curves of the $x \neq 0.4$ samples, shown in Fig. 7. Various points are worth noting. First, Fig. 6 exhibits two broad peaks, similar to the ones observed in Fig. 1(b), though now they are located at $T = 11.8(2) \text{ K}$, and $4.0(2) \text{ K}$; the fact that the peak locations are so close to the T_1 and T_2 events, signaled in Fig. 1(b), can hardly be regarded as fortuitous. Second, the absence of a frequency-dependent shift at T_1 indicates that this event is related to a transition from paramagnetism to long-range order. A closer look at the $\chi'_{ac}(T,$

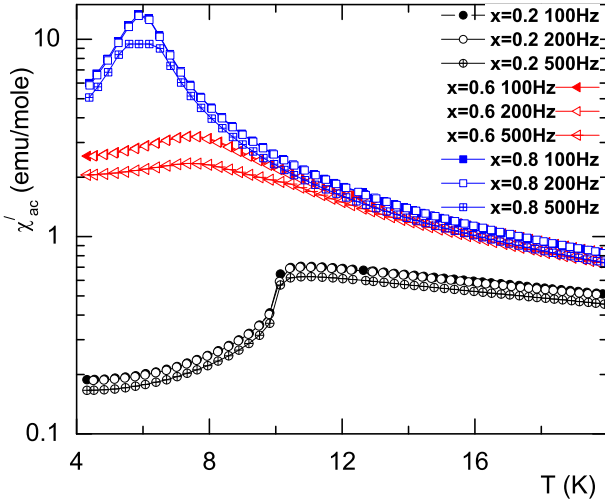


FIG. 7: (Color online) Thermal evolution of the zero- dc -field, real component of the ac susceptibility of the $x=0.2, 0.6$, and 0.8 samples, taken at 100, 200, and 500 Hz, with $h_{ac}=3$ to 5 Oe.

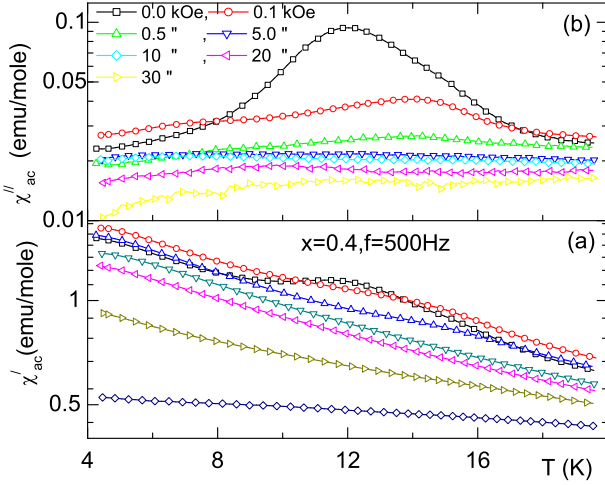


FIG. 8: (Color online) Thermal evolution of the isofield ac susceptibility of $x=0.4$ sample, taken at 500 Hz. The amplitude of the oscillating field is $h_{ac}=3\sim 5$ Oe while the range of the constant applied DC field H_{dc} is between 0 to 30 kOe. (a) χ''_{ac} : the out-of-phase component; (b) χ'_{ac} : the in-phase component.

$x \neq 0.4$) curves in Fig. 7 shows that the peak positions do not depend on the frequency, and that they occur at the same temperature as the maxima of $C(T, x \neq 0.4)$ and $M(T, x \neq 0.4)$ (see Table I); this adds credence to the association of T_1 with a magnetic transition. Third, the T_2 event only appears for the $x=0.4$ sample; further, the neutron diffractogram collected⁵ at $2\text{ K} < T_2$ indicates an ordered \vec{k}_2 mode. Therefore, the picture that emerges is that in this case the system suffers yet another transition at T_2 , occurring within the magnetically ordered phase.

Finally, Fig. 8 shows the influence of a non-zero dc field on the $x=0.4$ sample: we see that both χ'_{ac} and

χ''_{ac} are strongly affected even by a weak field, particularly near T_1 , when the asymmetric peak is strongly reduced, and a large portion of its intensity weight is shifted to higher temperatures as H is increased. This shift to higher temperature is yet another indication that ferromagnetic bonds are present in larger fractions, thus playing an important role at this Co concentration; one can therefore elect these couplings as the main mechanism behind the T_1 event.

D. Magnetoresistivity

In many cases, a reduction of $|\vec{\mu}|$ may be attributed to Kondo screening. Though it is not common that $|\vec{\mu}|$ of Tb^{3+} is reduced by such effect, we explored this possibility by checking whether there is a Kondo-type resistivity minimum for the $x=0.4$ sample. Representative resistivity curves, $\rho(T, H, x=0.4)$, are shown in Figs. 9 and 10. The high- T $\rho(T, H=0, x=0.4)$ curve [Fig. 9(a)] exhibits a metallic behavior with a linearity range that extends down to almost 50 K, below which a typical positive curvature sets in. Figures 9(b) and 9(c) indicate that at low temperatures the resistivity is dominated by the two events associated with the Gaussian peaks of the inset of Fig. 9(a). The intensity, shape, and position of each peak were found to depend on sample history, similar to what had already been noted for the magnetization isotherms. Based on our analysis of the $\chi_{dc}(T)$ and $\chi_{ac}(T)$ curves, these peaks are related to the T_1 and T_2 events, and, further, the observed shift in the peak positions (as compared to previously identified positions) is attributed to the different sensitivity of the resistivity probe.

The field dependence of $\rho(T, H, x=0.4)$ is best seen in Fig. 10(a). Both the upper inset of Fig. 10(a), as well as Fig. 10(b) indicate that the hysteresis effect is sharply decreased with temperature, in particular above T_1 . Moreover, the lower inset of Fig. 10(a) indicates that upon increasing H , $\rho(2\text{ K}, H, x=0.4)$ increases but surprisingly upon decreasing H , no corresponding decrease is observed in $\rho(T, H, x=0.4)$: this stands in sharp contrast to the expectation based on the features of Fig. 2(a); it suggests a field-induced metastable state with a longer relaxation time.

The observation that higher fields increase T_1 is an indication that the dominant couplings at T_1 are ferromagnetic; this confirms the findings drawn from the $\chi_{dc}(T, H, x=0.4)$ and $\chi_{ac}(T, f, H, x=0.4)$ studies. The intensity of the T_1 peak in some measurements is relatively strong, and, as a consequence, the total isofield resistivity curve exhibits a minimum situated well within the paramagnetic regime. Evidently this is not a Kondo minimum. Rather, based on the analysis of $\chi_{ac}(T, f, H, x=0.4)$, this is due to scattering from fluctuation processes accompanying the T_1 and T_2 events.

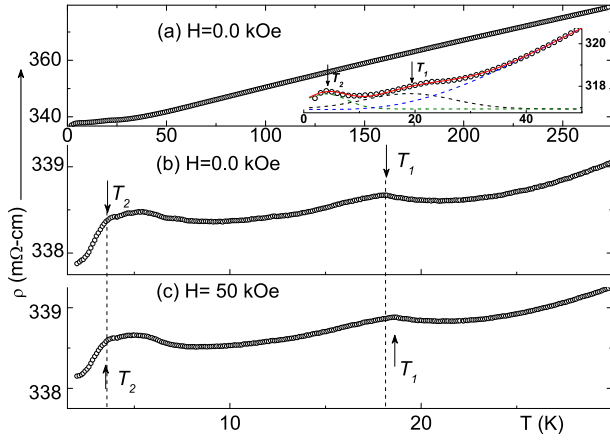


FIG. 9: (Color online) (a) Thermal evolution of the zero-field resistivity for the $x = 0.4$ sample. *Inset*: An example of decomposition of the low-temperature, zero-field resistivity curve into Gaussian contributions centered at T_1 and T_2 , and a conventional metallic Debye-Grüneisen contribution;²⁰ dashed lines represent these individual contributions, whose sum is shown as a (red) solid line. (b) Same as (a), but on an expanded scale. (c) Same as (b), but measured at 50 kOe. Vertical arrows denote the maxima of the T_1 and T_2 peaks, while dashed vertical lines compare T_1 and T_2 measured at $H = 0$ and 50 kOe.

IV. DISCUSSION AND CONCLUSIONS

It is worth noting that in spite of the above-mentioned layered geometry of the borocarbides crystal structure, numerous theoretical^{6–10} and experimental^{21–23} investigations emphasize the *three-dimensional* character of their electronic structure, transport, and magnetic properties. This is certainly the case for the present $\text{Tb}(\text{Co}_x\text{Ni}_{1-x})_2\text{B}_2\text{C}$ compositions; accordingly, this work considers the involved magnetic couplings to be isotropic.

A variation in the ratio of Ni/Co concentrations modifies the Fermi momentum which in turn alters the spatial scale of the RKKY oscillations, and, as a consequence, the magnetic couplings; the overall effect is that an x -dependent control of the magnetic properties is achieved.

Further insight into the evolution of these couplings can be gained if we separate the following three doping regimes: (i) In the $x = 0$ limit, the magnetic structure is a LSDW mode,^{24–26} resulting from dominant AFM couplings. On the other hand, its high-temperature CW behavior suggests the presence of subdominant FM couplings²² (similar features are evident in Fig.3); nonetheless, these cannot be attributed simply to an intralayer FM coupling, given the nature of the ensuing LSDW structure.^{24–26} (ii) For intermediate compositions, $0 < x < 1$, the dominant couplings for $x \leq 0.4$ are AFM, while they become FM for $x > 0.6$. (iii) In the $x = 1$ limit, the dominant couplings are FM.¹⁵ The picture that emerges from these observations is that both FM and AFM couplings are present in the whole $0 \leq x \leq 1$ range; however, the relative importance of

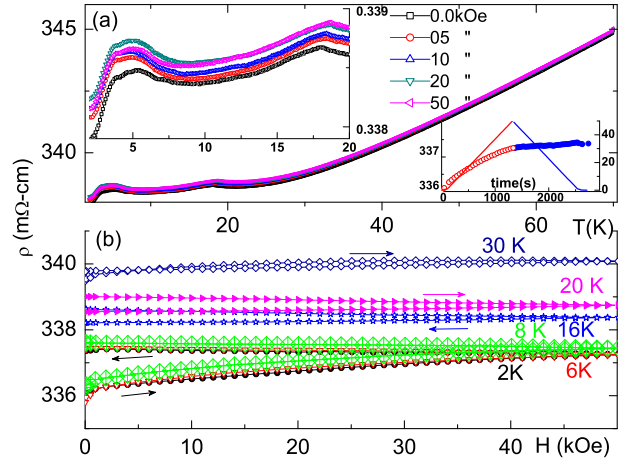


FIG. 10: (Color online) (a) Thermal evolution of isofield $\rho(T, H, x = 0.4)$ curves measured at various fields. *Upper left inset*: expansion of the low-temperature curves; *lower bottom inset*: $\rho(T = 2 \text{ K}, H, x = 0.4)$ (symbols) and applied field (solid lines) as a function of time showing the resistivity evolution on the increasing (open symbols) and decreasing (solid symbols) branch of the applied field. (b) Field-dependent $\rho(T, H, x = 0.4)$ isotherms measured at $T = 2, 6, 8, 16, 20, 30 \text{ K}$. The arrows denote the increasing or decreasing branch of H .

these couplings vary monotonically with x , being dominated by AFM bonds in the low- x limit while by FM bonds near the $x \rightarrow 1$ region.

This picture allows one to understand the non-linear evolution of $T_{cr}(x)$: for $x < 0.4$, the strength of the dominant AFM couplings are progressively reduced leading to a decrease in $T_N(x)$ with $\partial T_N / \partial x \simeq -18 \text{ K}/x$. On the other hand, for $x > 0.4$, the magnetic couplings are also reduced but, being predominantly FM, the rate of reduction of $T_C(x)$, $\partial T_C / \partial x \simeq -3 \text{ K}/x$, is almost one sixth of the value found for the $x < 0.4$ samples.

For the particular $x = 0.4$ case, both ferromagnetic and antiferromagnetic couplings are assumed to be present with almost equal strength. Furthermore, their competitive and opposing tendencies give rise to two magnetic events which are manifested as (i) a disorder-to-order transition at T_1 , and (ii) an order-to-order transformation at T_2 . Experimental manifestation of the T_2 process is evident in all measurements: as a peak in $\chi_{dc}(T)$, $\chi_{ac}(T, f, H)$, and $\rho(T, H)$, as a surge of a \vec{k}_2 mode in neutron diffraction, and as a shoulder in $C(T)$. By contrast, since the event at T_1 is assumed to be accompanied by a weak energy of transformation, then its observation depends on the probing technique; specifically, it is evident in $\chi_{dc}(T)$, $\chi_{ac}(T, f, H)$, and $\rho(T, H)$ but, depending on the involved frequency window, it appears at different temperatures.

Finally, for $x = 0.4$, the moment reduction (as seen by the neutron diffraction below T_2) and the strong low-temperature deviation from the CW extrapolation (as seen by $\chi_{dc}(T)$ below 150 K) are unexpected. It is worth

recalling that (i) an application of a magnetic field leads to a full moment saturation at 2 K, accompanied by a metastable state, (ii) the evolution of the 50 and 90 kOe induced magnetic moment is smooth, and with no sign of anomalies, at or below T_1 and T_2 , and that (iii) the Brillouin function is almost followed for $T > T_1$. A Kondo screening, or magnetic fluctuations, could in principle provide possible mechanisms for the moment reduction; however, our resistivity results exclude any influence of a Kondo screening, while the observation of the T_1 event in $\chi_{dc}(T)$ rules out any significant role played by magnetic fluctuations. Spin glass features²⁷ could also be invoked, given that $\chi_{ac}(T, f)$ exhibits a small, but noticeable frequency-dependent shift-in-temperature (see the inset of Fig. 6); however, these should also be discarded, since neutron diffraction indicates well ordered magnetic and crystalline structures. The observation that CW behavior is recovered above 150 K is a strong indication that the above mentioned anomalies are related to CEF configurations. In the absence of an applied magnetic field, they modify the level scheme of the free Tb^{3+} ion in such a way that the zero-field moment is strongly reduced, the CW behavior is disrupted below 150 K, and strong hysteresis and relaxation effects are induced. An applied magnetic field re-arranges the CEF-split levels in such a way that the moment is restored to the values observed in neighboring compositions, the CW behavior survives to much lower temperatures, and hysteresis

effects are reduced.

In summary, the x -dependent evolution of the thermodynamic properties of $\text{Tb}(\text{Co}_x\text{Ni}_{1-x})_2\text{B}_2\text{C}$ was investigated by a wide range of experimental techniques. The magnetic properties across the whole concentration range have been found to be consistent with the findings of the neutron diffraction studies: in particular, the dominant magnetic couplings for $x \leq 0.4$ composition are found to be AFM (in agreement with the observed AFM modes), while those, for $x > 0.6$, are strongly FM (also in agreement with the observed FM modes). Furthermore, the magnetic transition temperatures, as well as the Tb magnetic moments are observed to evolve non-monotonically with the Ni/Co ratio. These unexpected features are highly emphasized in the anomalous behavior of the $x = 0.4$ sample, which, in addition, exhibits a zero-field moment reduction and a surge of two magnetic events (argued to be related to disorder-to-order and an order-to-order transitions). These features are attributed to combined influences of competing magnetic couplings and crystalline electric field effects.

Acknowledgments

Partial financial support from the Brazilian Agencies CNPq, CAPES, and FAPERJ is gratefully acknowledged.

-
- ¹ K.-H. Müller and V. N. Narozhnyi, Rep. Prog. Phys. **64**, 943 (2001).
 - ² L. C. Gupta, Adv. Phys. **55**, 691 (2006).
 - ³ B. K. Cho, P. C. Canfield, and D. C. Johnston, Phys. Rev. Lett. **77**, 163 (1996).
 - ⁴ P. C. Canfield, P. L. Gammel, and D. J. Bishop, Phys. Today **51**, 40 (1998).
 - ⁵ M. ElMassalami, H. Takeya, B. Ouladdiaf, R. Maia Filho, A. M. Gomes, T. Paiva, and R. R. dos Santos, Phys. Rev. B **85**, 174412 (2012).
 - ⁶ W. E. Pickett and D. J. Singh, Phys. Rev. Lett. **72**, 3702 (1994).
 - ⁷ L. F. Matthias, Phys. Rev. B **49**, 13279 (1994).
 - ⁸ P. Ravindran, B. Johansson, and O. Eriksson, Phys. Rev. B **58**, 3381 (1998).
 - ⁹ J. I. Lee, T. S. Zhao, I. G. Kim, B. I. Min, and S. J. Youn, Phys. Rev. B **50**, 4030 (1994).
 - ¹⁰ R. Coehoorn, Physica C **228**, 331 (1994).
 - ¹¹ J. Y. Rhee, X. Wang, and B. N. Harmon, Phys. Rev. B **51**, 15585 (1995).
 - ¹² P. R. Bertussi, A. L. Malvezzi, T. Paiva, and R. R. dos Santos, Phys. Rev. B **79**, 220513 (2009).
 - ¹³ T. Paiva, M. El Massalami, and R. R. dos Santos, J. Phys.: Condens. Matter **15**, 7917 (2003).
 - ¹⁴ J. W. Lynn, S. Skanthakumar, Q. Huang, S. K. Sinha, Z. Hossain, L. C. Gupta, R. Nagarajan, and C. Godart, Phys. Rev. B **55**, 6584 (1997).
 - ¹⁵ M. ElMassalami, R. Moreno, R. M. Saeed, F. A. B. Chaves, C. M. Chaves, R. E. Rapp, H. Takeya, B. Ouladdiaf, and M. Amara, J. Phys: Condens Matter **21**, 216006 (2009).
 - ¹⁶ B. K. Cho, P. C. Canfield, and D. C. Johnston, Phys. Rev. B **53**, 8499 (1996).
 - ¹⁷ M. ElMassalami, M. Amara, R.-M. Galera, D. Schmitt, and H. Takeya, Phys. Rev. B **76**, 104410 (2007).
 - ¹⁸ C. Song, Z. Islam, L. Lottermoser, A. I. Goldman, P. C. Canfield, and C. Detlefs, Phys. Rev. B **60**, 6223 (1999).
 - ¹⁹ C. Song, D. Wermeille, A. I. Goldman, P. C. Canfield, J. Y. Rhee, and B. N. Harmon, Phys. Rev. B **63**, 104 507 (2001).
 - ²⁰ P. B. Allen, in *Quantum Theory of Real Materials*, edited by J. R. Chelikowsky and S. G. Louie (Kluwer, Boston, 1996), p. 319.
 - ²¹ R. J. Cava, H. Takagi, H. W. Zandbergen, J. J. Krajewski, W. F. Peck Jr., T. Sigerist, B. Batlogg, R. B. V. Dover, R. J. Felder, K. Mizuhashi, et al., Nature **367**, 254 (1994).
 - ²² H. Eisaki, H. Takagi, R. J. Cava, B. Batlogg, J. J. Krajewski, W. F. Peck, K. Mizuhashi, J. O. Lee, and S. Uchida, Phys. Rev. B **50**, R647 (1994).
 - ²³ H. Schmidt and H. F. Braun, Physica C **229**, 315 (1994).
 - ²⁴ H. Kawano-Furukawa, H. Tsukagoshi, T. Nagata, C. Kobayashi, H. Yoshizawa, and H. Takeya, Phys. Rev. B **77**, 144426 (2008).
 - ²⁵ P. Dervenagas, J. Zarestky, C. Stassis, A. I. Goldman, P. C. Canfield, and B. K. Cho, Physica C **212**, 1 (1995).
 - ²⁶ P. Dervenagas, J. Zarestky, C. Stassis, A. I. Goldman, P. C. Canfield, and B. K. Cho, Phys. Rev. B **53**, 8506 (1996).
 - ²⁷ J. A. Mydosh, J. Magn. Magn. Mater. **157-158**, 606 (1996).